JOURNAL OF MATERIALS SCIENCE **40** (2005) 2837–2842

Effect of pH on crystallization of sputtered hydroxyapatite film under hydrothermal conditions at low temperature

K. OZEKI*, H. AOKI, Y. FUKUI
Frontier Research and Development Center, Tokyo Denki University, Ishizaka, Hatoyama, Hiki, Saitama 350-0394, Japan
E-mail: ozeki@frontier.dendai.ac.jp

Hydroxyapatite (HA) was coated onto titanium substrates using radio frequency sputtering, and the as-sputtered films were placed under hydrothermal conditions in distilled water solutions at pH 5.0, 7.0 and 9.0 and 110°C. The crystallinity, the Ca/P ratio, thickness, and the surface of the films were observed using XRD, EDS, and SEM, respectively.

The as-sputtered film was crystallized in distilled water at varying pH after the hydrothermal treatment, and the crystallinity of the film increased with treatment time. The HA crystal size increased with pH. At pH 5.0, β-TCP was produced as well as HA. The Ca/P ratio of the film decreased with increasing treatment, and the ratio at pH 9.0 was 1.74 after 48 h, while in pH 5.0 and 7.0 it was 1.63. After hydrothermal treatment, the film remnant ratio increased with pH, with 75.9, 82.4 and 91.7% of the film remaining after 48 h at pH 5.0, 7.0 and 9.0, respectively.

1. Introduction

Plasma spraying techniques are used to coat hydroxyapatite ($Ca_{10}(PO_4)_6(OH)_2$; HA) onto metal for biomaterials such as dental implants and artificial joints. However, the resultant HA coating is brittle because the coating is more than 50 μm in thickness, with low density [1]. As an alternative, a radio frequency (RF) sputtering technique has been investigated as a method to obtain HA films less than 1 μm thick [2–5]. However, the sputtered HA film has low crystallinity, and has Ca/P ratios higher than the 1.67 of stoichiometric HA, due to the inclusion CaO, which is cytotoxic [6–8]. The low crystallinity accelerates the speed of dissolution of the HA film in the living body, and this high rate of dissolution leads to the disappearance of films that bond to bone tissue at an early stage after implantation [9–11]. Cooley *et al.* reported that HA sputtered film around titanium implants was lost after 3 weeks of implantation [12]. Appropriate heat treatment can improve the dissolution properties by crystallizing the film. The crystallization of sputtered HA films needs high temperature, e.g. over 600°C in air [13], and conventional heat treatment in an electric furnace leads to films that tend to degrade and easily form cracks between the film and the titanium substrate because of differences in thermal expansion and the formation of TiO_2 [14]. Therefore, it is necessary to crystallize the film at low temperature. A hydrothermal technique has been used for synthesis of HA at less than 350°C [15–17].

In a previous paper it was reported that sputtered HA film could be crystallized in an electrolyte solution containing Ca and P at 110°C using a hydrothermal technique, without degradation of the film [18]. In pullout tests using explanted femora from beagle dogs, the crystallized film had 1.6 times higher bone bonding strength than the plasma spray coating after 12 weeks of implantation. The electrolyte solution was used to lower the dissolution of the sputtered film during the hydrothermal treatment; however, the solution would also inhibit HA crystal growth. In the present study, the sputtered film was crystallized in distilled water at varying pH during the hydrothermal treatment. After the treatment, the films were investigated using X-ray diffractometry (XRD), energy dispersive X-ray spectroscopy (EDS) and scanning electron microscopy (SEM).

2. Materials and methods

2.1. Materials

The substrates used were titanium plates (10 × 10 × 1 mm^2). The surface roughness of the substrates (R_a) was 1.0 ± 0.1 μm ($N = 10$). HA powder (Ube Materials Corp., Japan) was used for the sputtering target, and the HA was heated to 900°C for 1 h. The particle size was 2–10 μm.

2.2. Methods

2.2.1. Preparation of HA films on titanium

RF magnetron sputtering was carried out using an L-210HS-F (ANELVA Corp.) chamber. The distance

*Author to whom all correspondence should be addressed.

between the target and the substrate was about 60 mm, and the diameter of the target was 50 mm. Both the target and the substrate were water-cooled during the sputtering process. The sputtering chamber was evacuated to a pressure below 1×10^{-5} Pa using an oil-diffusion pump with a liquid nitrogen trap. Ar gas (99.999%) was then introduced into the chamber by means of a mass flow controller. Before deposition took place, the target was pre-sputtered using Ar ions for 10 min, with the substrate covered with a shield. The procedure to obtain films 1 μm thick was carried out at an Ar pressure of 0.5 Pa and a discharge power of 100 W.

2.2.2. Hydrothermal treatment

Hydrothermal treatment was carried out in distilled water at 110°C and 0.145 MPa using an autoclave. The pH of the distilled water used as the hydrothermal solution was adjusted to 5.0, 7.0 and 9.0 with NaOH/HCl. Twenty-five plates were placed in 500 ml of the each solution during the treatment. The treatment times selected were 6, 12, 24, 48 and 72 h.

After the hydrothermal treatment, each plate was identified using XRD (RINT2000; Rigaku Corp.) with a CuKα radiation source operating at 40 kV and a 40 mA excitation current. Surface observation and elemental analysis of the films were carried out using SEM (JSM-5310LVB; JEOL) and EDS (JED-2140; JEOL) with an accelerating voltage of 20 kV. The (Ca + P)/Ti atomic ratio of the samples was analyzed before and after the hydrothermal treatment using the ZAF method by EDS, with an accelerating voltage of 20 kV. The film thickness was calculated from a calibration curve of the (Ca+P)/Ti ratio versus film thickness, and the percentage remnant film thickness was calculated by dividing the remnant film thickness by the initial film thickness. The initial film thickness on all plates was determined to be 1.0–1.2 μm. The Ca/P ratio of the films was also calculated using EDS, and the final result was obtained from the average of five samples.

3. Results and discussion

3.1. XRD and SEM observations of the sputtered films after hydrothermal treatment in pH 9.0 solution

Fig. 1 shows XRD patterns of an HA target and an as-sputtered film on titanium. Fig. 1a shows highly crystalline HA in the target. In Fig. 1b, a broad peak was observed at around $2\theta = 31°$, corresponding to non-crystalline HA; in addition, three strong titanium peaks were observed at $2\theta = 35.1°$, 38.4° and 40.1°. Fig. 2 shows XRD patterns of the films with varying treatment time at pH 9.0. The number of sharp HA peaks (∇) increased with treatment time. A sharp peak appeared at $2\theta = 25.8°$ corresponding to the (002) plane, after 6 h, then a peak at the (112) plane appeared at $2\theta = 32.2°$ after 24 h. The (002) plane peak decreased with treatment time. Fig. 3 shows the intensity ratio of the (002) and (300) HA planes in the XRD patterns as a function of the treatment time. The I_{002}/I_{300} of standard hydroxyapatite (JCPDS No.9–432) is 0.67. The ratio was 2.4 after 6 h and decreased to 0.73 after 72 h,

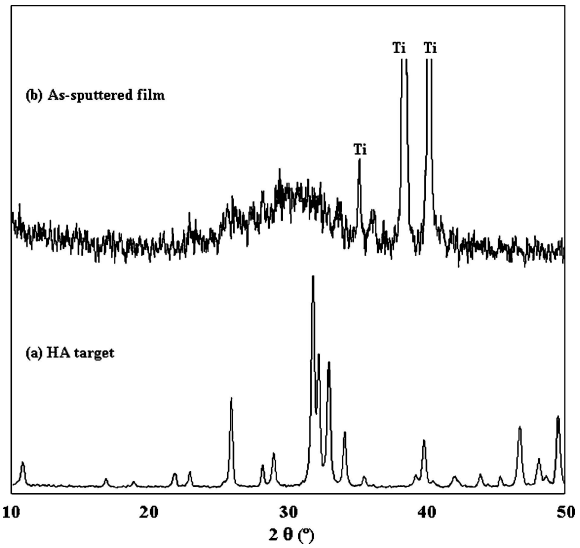

Figure 1 XRD patterns of: (a) the HA target used for sputtering and (b) an as-sputtered film. Key: Ti = titanium substrate.

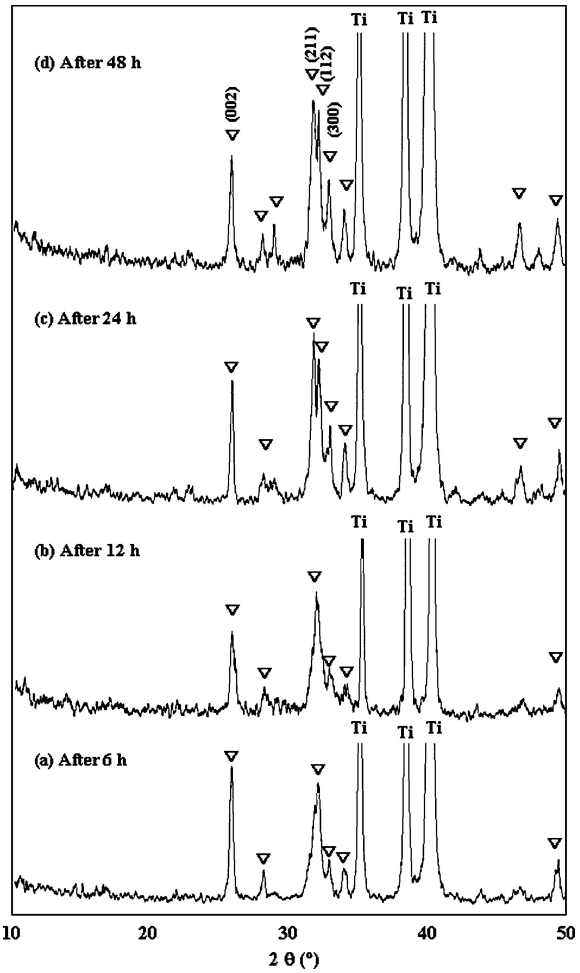

Figure 2 The XRD patterns of the sputtered films after hydrothermal treatment. Key: ∇ = HA.

close to 0.67. This indicates that HA crystals preferentially grew along the *c*-axis early in the reaction, then grew preferentially along the *a*-axis, which correspond with the HA crystals growing from needle-like shapes to flat-hexagonal shapes.

Fig. 4 shows SEM photos of the sputtered films with varied treatment times at pH 9.0. Needle-like HA crystals 0.2–0.3 μm in width and 1–2 μm in length

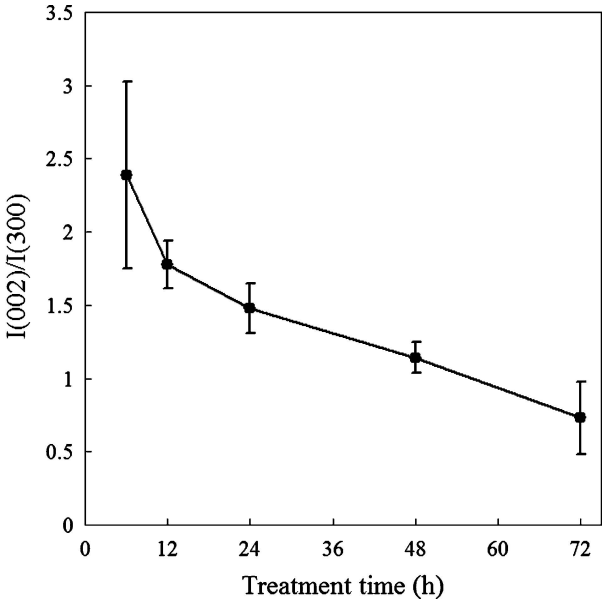

Figure 3 Intensity of the 002 and 300 planes of hydroxyapatite in the XRD pattern of the sputtered films as a function of hydrothermal treatment time ($N = 5$).

were observed after 6 h, then, after 12 h, some flat hexagonal HA crystals 1–1.5 μm in width and 2–3 μm in length grew. After 24 h, all parts of the surface were covered by flat hexagonal HA crystals. This SEM result corresponds with the decrease in I_{002}/I_{300} ratio with treatment time (Fig. 3). Ban *et al.* also reported in HA deposition using a hydrothermal electrochemical method, and the *c*-axis/*a*-axis of the needle-like apatite decreased with increasing treatment time [15].

In general, HA crystal preferentially grows along the *c*-axis. The probability of deposition in the *c*-plane is higher than in the *a*-plane because the *c*-axis is considerably smaller than the *a*-axis in HA crystals. The lattice constants of HA are $a = 0.9418$ nm and $c = 0.6884$ nm [1, 7]. Onuma *et al.* explained the *c*-axis preferential crystal growth of HA using a cluster growth model in which clusters of $Ca_9(PO_4)_6$ deposit along the *c*-axis binding Ca(1) as a centre [19]. Then the preferential crystal growth changes from the *c*-axis to the *a*-axis to maintain its surface energy at an upper limit because the surface energy of the crystal increases with height of deposition along the *c*-axis.

3.2. XRD and SEM observation of the sputtered films after hydrothermal treatment in solutions of varying pH

Fig. 5 shows the XRD patterns of the film in solutions at pH 5.0, 7.0, and 9.0 after 24 h hydrothermal treatment. At pH 9.0, six strong HA peaks (∇) were clearly observed at $2\theta = 10.8$, 25.9, 31.8, 32.2, 32.9, and 34.0°. When the pH was lowered, the peaks became broader. At pH 5.0, three peaks additional to the HA peaks appeared at $2\theta = 10.9$, 25.8 and 27.8°, corresponding to β-TCP (▼).

Fig. 6 shows the pH changes in the pH 5.0, 7.0, and 9.0 solutions with treatment time. In the pH 9.0 solution, the pH value was almost constant between pH 8.88 and 9.12. However, in the pH 7.0 and 5.0 solutions, the pH value rapidly rose to pH 8.03 and 7.15, respectively, after 6 h, because of dissolution of CaO from the as-sputtered film. Lucas *et al.* and Ozeki *et al.* reported

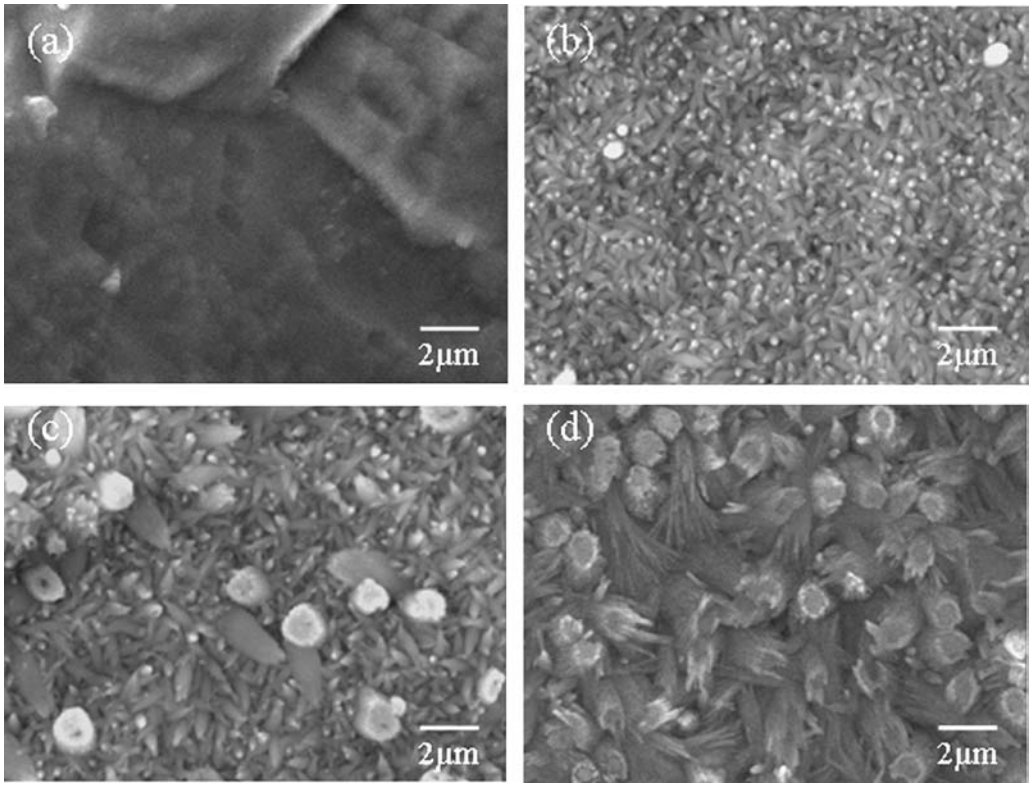

Figure 4 SEM photographs of the sputtered films: (a) before, and (b) 6, (c) 12, and (d) 24 h after being subjected to the hydrothermal treatment.

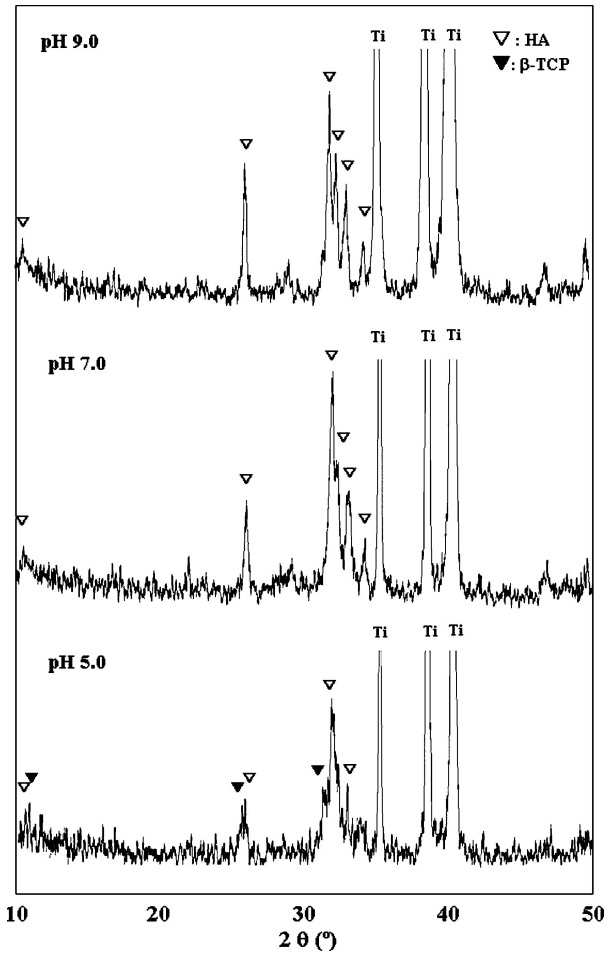

Figure 5 The XRD patterns of the sputtered films after the hydrothermal treatment for 24 h in solutions at pH 5.0, 7.0, and 9.0, Key: ∇ = HA, $\blacktriangledown$ = β-TCP.

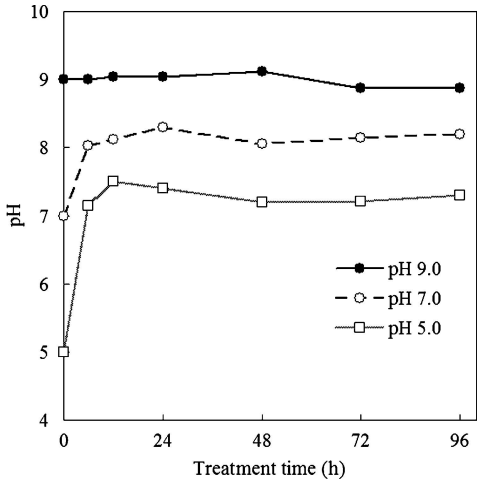

Figure 6 pH of each solution (pH 5.0, 7.0, 9.0) as a function of the hydrothermal treatment time.

that as-sputtered films from HA targets include CaO as well as HA [6, 7]. The pH value was highest after 12 or 24 h, and slightly decreased after that due to absorption of CO_2 from the air.

Fig. 7 shows the Ca/P ratio of the film in the pH 5.0, 7.0, and 9.0 solutions. The initial Ca/P ratio was 2.03, more than the 1.68 of stoichiometric HA due to the CaO, as shown in Fig. 6. In the pH 9.0 solution, the Ca/P ratio decreased, and remained at 1.74 after 48 h.

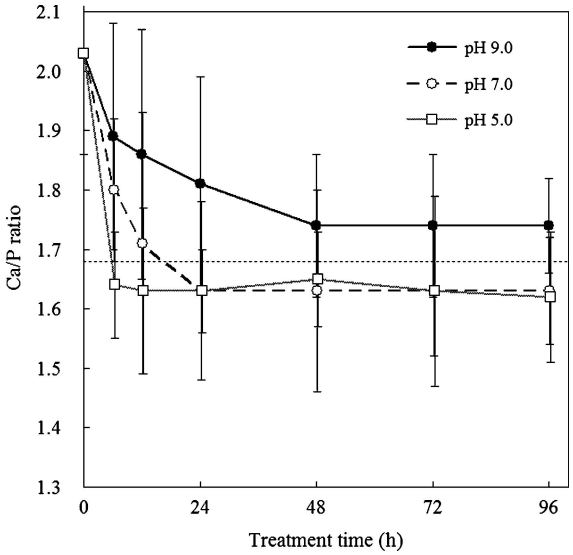

Figure 7 Ca/P ratios of the sputtered films in pH 5.0, 7.0, 9.0 solutions as a function of the hydrothermal treatment time (N = 54). The dotted line indicates Ca/P = 1.68.

The Ca/P ratio decreased with diffusion of CaO into the solution because CaO has high solubility. A film with a Ca/P ratio of 1.74 can be calculated to include 2.5 wt% of CaO. At pH 7.0 and 5.0, the Ca/P ratio remained at 1.63 after 24 and 12 h, respectively, a value that is lower than 1.68. During the hydrothermal treatment, the as-sputtered film was crystallized by repeated dissolution and recrystallization. At pH 7.0 and 5.0, β-TCP ($\blacktriangledown$) as well as HA (∇) can be crystallized. From Fig. 5, from the XRD pattern, β-TCP was also observed in the pH 5.0 solutions. Films that have a Ca/P ratio of 1.63 would include 28% TCP because the Ca/P ratio of TCP is 1.5. Together, this indicates that dissolved Ca and P ions from the sputtered film were recrystallized to β-TCP in acid solution. β-TCP is prepared at pH 4–7 in wet methods [1]. Bouler *et al.* studied the influence of pH on synthesis of HA and β-TCP from hydrolyzed dicalcium phosphate dihydrate solutions. They showed that the ratio of β-TCP to HA increases with decreasing pH and that 100% β-TCP can be synthesized below pH 6.98 [20].

Fig. 8 shows SEM photos of the sputtered films after the 24 h treatment in solutions at pH 5.0, 7.0, and 9.0. In pH 9.0 solution, flat hexagonal HA crystals, as seen in Fig. 4, were observed (Fig. 8d). The size of the HA crystals decreased with pH, and they were less than 0.1 μm at pH 5.0 (Fig. 8b). A driving force of crystal growth is the degree of supersaturation. The degree of supersaturation decreases with pH because the solubility of calcium phosphates increases with decreasing pH [21–23]. Consequently, HA crystal growth rate decreases with pH.

3.3. Thickness of the sputtered films after hydrothermal treatment at varying pH

Fig. 9 shows remnant film thickness to initial film thickness ratios with treatment times at pH 5.0, 7.0, and 9.0. In all solutions, the ratio dropped after 6 h, and become stable after 48 h. These ratios were 75.9, 82.4

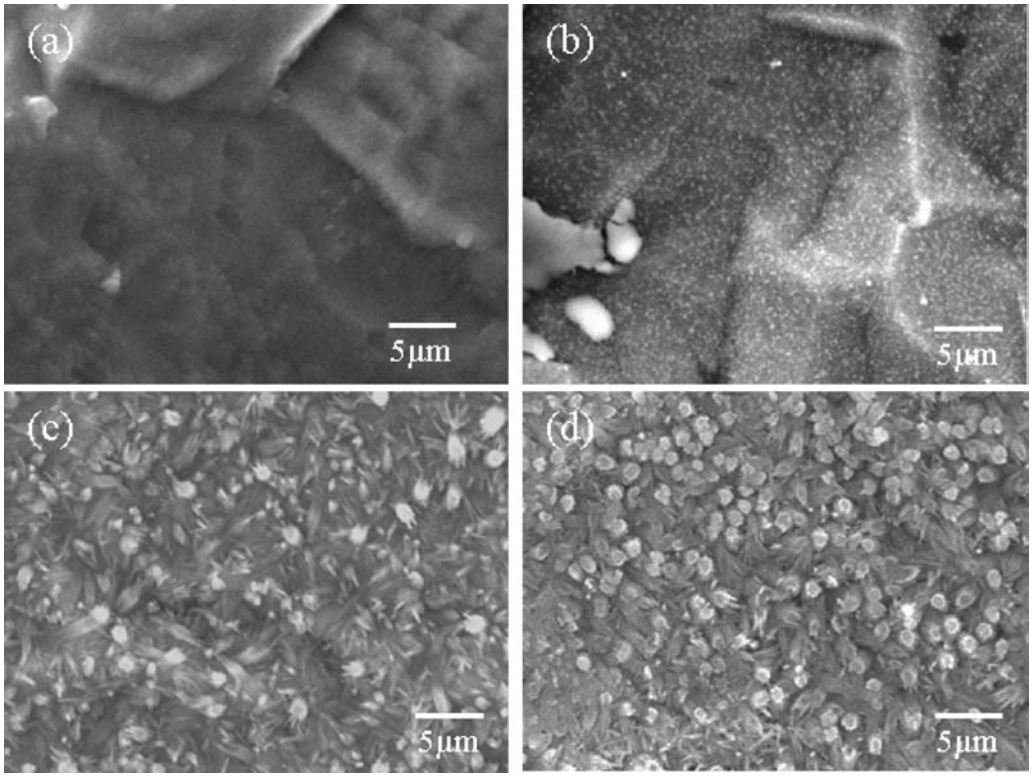

Figure 8 SEM photographs of the sputtered films: (a) before, and after being subjected to the hydrothermal treatment for 24 h at (b) pH 5.0 (c) 7.0, and (d) 9.0.

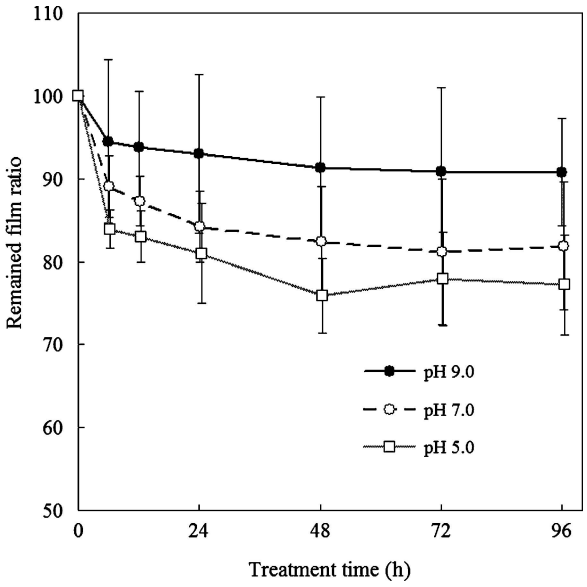

Figure 9 Remnant film ratios of the sputtered films at pH 5.0, 7.0, 9.0 as a function of the hydrothermal treatment time ($N = 5$).

and 91.7% at pH 5.0, 7.0 and 9.0, respectively. The ratio decreased with pH values. The pH 9.0 solution suppressed dissolution of the film during the treatment because of the low solubility of HA at this pH, even at high temperature. Zhang *et al.* reported that the dissolution of HA varied with solution pH at 200°C. The dissolution of HA at pH 5.0 and 7.0 is about 2.0 and 1.4 times higher, respectively, than that at pH 9.0 [24].

The sputtered HA film has high solubility because of its low crystallinity. The film completely dissolves in physiological saline (0.9% NaCl) at 37°C within 24 h [18]. Ohtsuka *et al.* also reported that the HA film dissolved within 1 day in Hank's solution [25]. In the present study, we suppressed the dissolution of the film by lowering the solubility of the HA using a hydrothermal technique. The solubility of calcium phosphates decreased with solution temperature. The relationship between solubility and solution temperature is given by $\log Ks = -8219.41/T - 1.6657 - 0.09825T$ [26]. From this equation, the solubilities, *Ks*, are 3.16×10^{-59} and 2.304×10^{-59} mol/L at 0 and 37°C, respectively. Ks decreased with the solution temperature, and reached 1.75×10^{-61} mol/L at 110°C.

From above results, for less dissolution of the film and thus successful application to biomaterials, the as-sputtered film has to be recrystallized by hydrothermal treatment in a pH 9.0 solution. The treatment time needs to be greater than 48 h to obtain the appropriate Ca/P ratio in the film, slightly higher than stoichiometric HA. Lastly, the film must be immersed in distilled water or saline to remove any CaO.

4. Conclusions

As-sputtered films were crystallized in distilled water at varying pH by hydrothermal treatment, and the crystallinity of the film increased with treatment time. The HA crystal size increased with pH. At pH 5.0, β-TCP as well as HA was identified from XRD pattern. The Ca/P ratio of the film decreased with the treatment time, and the Ca/P ratio at pH 9.0 was 1.74 after 48 h, and 1.63 at pH 5.0 and 7.0. The remnant film ratio increased with pH, and 75.9, 82.4 and 91.7% remained after a 48 h treatment time at pH 5.0, 7.0 and 9.0, respectively.

Acknowledgements

The authors would like to thank Dr. A. Ito (National Institute of Advanced Industrial Science and Technology, Japan) for stimulating discussions about the HA crystal growth theory.

References

1. H. AOKI, "Medical applications of hydroxyapatite" (Ishiyaku EuroAmerica, Inc, St. Louis, 1994).
2. J. A. JANSEN, J. G. C. WOLKE, S. SWANN, J. P. C. M. VAN DER WAERDEN and K. DE GROOT, *Clin. Oral. Impl. Res.* **4** (1993) 28.
3. K. OZEKI, T. YUHTA, H. AOKI, I. NISHIMURA and Y. FUKUI, *J. Mater. Sci. Mater. Med.* **13** (2002) 253.
4. T. HAYAKAWA, M. YOSHINARI, K. NEMOTO, J. G. C. WOLKE and J. A. JANSEN, *Clin. Oral. Impl. Res.* **11** (2000) 296.
5. J. E. G. HULSHOFF, T. HAYAKAWA, K. VAN DIJK, A. F. M. LEIJDEKKERS-GOVERS, J. P. C. M. VAN DER WAERDEN and J. A. JANSEN, *J. Biomed. Mater. Res.* **36** (1997) 75.
6. L. C. LUCAS, W. R. LACEFIELD, J. L. ONG and R. Y. WHITEHEAD, *Colloids and Surface A: Physiochemical and Engineering Aspects* **77** (1993) 141.
7. K. OZEKI, T. YUHTA, H. AOKI, I. NISHIMURA and Y. FUKUI, *Bio-Med. Mat. Eng.* **10** (2000) 221.
8. K. OZEKI, T. YUHTA, Y. FUKUI and H. AOKI, *Surface and Coatings Technology* **160** (2002) 54.
9. J. G. C. WOLKE, K. DE GROOT and J. A. JANSEN, *J. Biomed. Mater. Res.* **39** (1998) 524.
10. E. M. BURKE, J. D. HAMAN, J. J. WEIMER, A. B. CHENEY, J. M. RIGSBEE and L. C. LUCAS, *J. Biomed. Mater. Res.* **57** (2001) 41.
11. K. OZEKI, T. YUHTA, H. AOKI, I. NISHIMURA and Y. FUKUI, *Bio-Med. Mater. Eng.* **11** (2001) 63.
12. D. R. COOLEY, A. F. VAN DELLEN, J. O. BURGESS and A. S. WINDELER, *J. Prosthet. Dent.* **67** (1992) 67.
13. K. VAN DIJK, H. G. SCHAEKEN, J. G. C. WOLKE and J. A. JANSEN, *Biomater.* **17** (1996) 405.
14. M. YOSHINARI, T. HAYAKAWA, J. G. C. WOLKE, K. NEMOTO and J. A. JANSEN, *J. Biomed. Mater. Res.* **37** (1997) 60.
15. S. BAN and S. MARUO, *J. Biomed. Mater. Res.* **42** (1998) 387.
16. R. E. RIMAN, W. L. SUCHANEK, K. BYRAPPA, CHUN-WEI CHEN, P. SHUK and C. S. OAKES, *Solid State Ionics* **151** (2002) 393.
17. M. YOSHIMURA, P. SUJARIDWORAKUN, F. KOH, T. FUJIWARA, D. PONGKAO and A. AHNIYAZ, *Mater. Sci. Eng. C* **24** (2004) 521.
18. K. OZEKI, A. MISHIMA, T. YUHTA, Y. FUKUI and H. AOKI, *Bio-Med. Mater. Eng.* **13** (2003) 451.
19. K. ONUMA and A. ITO, *Chem. Mater.* **10** (1998) 3346.
20. J. M. BOULER, R. Z. LEGEROS and G. DACULSI, *J. Biomed. Mater. Res.* **51** (2000) 680.
21. CHRISTEL P. A. T. KLEIN, J. M. A. DE BLIECK-HOGERVORST, J. G. C. WOLKE and K. DE GROOT, *Biomater.* **11** (1990) 509.
22. M. R. CHRISTOFFERSEN, J. CHRISTOFFERSEN and J. ARENDS, *J. Cryst. Growth* **67** (1984) 107.
23. E. VALSAMI-JONES, K. V. RAGNARSDOTTIR, A. PUTNIS, D. BOSBACH, A. J. KEMP and G. GRESSEY, *Chem. Geol.* **151** (1998) 215.
24. H. ZHANG, S. LI and Y. YAN, *Ceram. Int.* **27** (2001) 451.
25. Y. OHTSUKA, M. MATSUURA, N. CHIBA, M. YOSHINARI, T. SUMII and T. DERAND, *Surf. and Coat. Tech.* **65** (1994) 224.
26. J. C. ELLIOT, "Structure and chemistry of apatites and other calcium orthophosphates" (Elsevier Science Publishers, Amsterdam, 1994) p. 157.

Received 16 November 2004
and accepted 4 February 2005